

ARTICLE

Open Access

Loss of CYLD accelerates melanoma development and progression in the Tg(*Grm1*) melanoma mouse model

Miriam Martha de Jel¹, Mandy Schott¹, Susanne Lamm¹, Winfried Neuhuber², Silke Kuphal¹ and Anja-Katrin Bosserhoff¹ 

Abstract

The deubiquitinase cylindromatosis (CYLD) is a well-known tumor suppressor, found to be down regulated in many cancer types including breast cancer, colon carcinoma and malignant melanoma. CYLD is suppressed in human melanoma cells by the transcriptional repressor SNAIL1 leading to an increase of their proliferative, invasive and migratory potential. To gain additional insights into the distinct function of this tumor suppressor gene a new mouse model Tg(*Grm1*)*Cyld*^{-/-} was generated. Herewith, we demonstrate that *Cyld*-deficiency leads to earlier melanoma onset and accelerated tumor growth and metastasis in the GRM1 melanoma mouse model. First, RNA sequencing data revealed a potential role of CYLD in the regulation of genes involved in proliferation, migration and angiogenesis. Experiments using cell lines generated from both primary and metastatic melanoma tissue of Tg(*Grm1*) *Cyld*^{-/-} and Tg(*Grm1*) *Cyld*^{+/+} mice confirmed that loss of CYLD enhances the proliferative and migratory potential, as well as the clonogenicity in vitro. Moreover, we could show that *Cyld*-knockout leads to increased vasculogenic mimicry and enhanced (lymph-) angiogenesis shown by tube formation assays, immunohistochemistry and mRNA expression analyses. In summary, our findings reveal new functional aspects of CYLD in the process of (lymph-) angiogenesis and demonstrate its importance in the early process of melanoma progression.

Introduction

The tumor suppressor function of cylindromatosis (CYLD) was first described in the disease of familial cylindromatosis, a rare benign tumor of skin appendages¹. Since then, both depletion and mutation of CYLD have been associated with development and progression of a variety of tumors such as cancer of the breast, colon and lung²⁻⁴. CYLD was also shown to be suppressed on mRNA, as well as protein level in human cell lines and tissue samples of malignant melanoma⁵⁻⁷. Melanoma represents the most aggressive form of skin cancer with

still increasing incidence rates. Here, CYLD expression is down regulated in consequence of elevated SNAIL1 expression, resulting in augmented CyclinD1 and N-Cadherin levels⁵ and in an increase in proliferation, migration and invasion of human melanoma cells. Furthermore, CYLD expression was shown to be inversely correlated with overall and progression-free survival in melanoma patients⁵. On a molecular level, the deubiquitinase CYLD regulates several important signaling pathways as the NF- κ B, JNK and Wnt/ β -Catenin pathway⁸⁻¹⁰.

In this study, we analyzed the role of CYLD for the first time in a murine model for spontaneous melanoma development. Tg(*Grm1*) mice display pigmented lesions after a short latency and with complete penetrance¹¹. GRM1 is a seven transmembrane domain comprising G-protein coupled receptor whose expression was shown to be up-regulated in human melanoma cell lines and tissues

Correspondence: Anja-Katrin Bosserhoff (anja.bosserhoff@fau.de)

¹Institute for Biochemistry, University of Erlangen-Nürnberg (FAU), Erlangen, Germany

²Institute for Anatomy, University of Erlangen-Nürnberg (FAU), Erlangen, Germany

These authors contributed equally: Miriam Martha de Jel, Mandy Schott
These authors contributed equally: Silke Kuphal, Anja-Katrin Bosserhoff

© The Author(s) 2019



Open Access This article is licensed under a Creative Commons Attribution 4.0 International License, which permits use, sharing, adaptation, distribution and reproduction in any medium or format, as long as you give appropriate credit to the original author(s) and the source, provide a link to the Creative Commons license, and indicate if changes were made. The images or other third party material in this article are included in the article's Creative Commons license, unless indicated otherwise in a credit line to the material. If material is not included in the article's Creative Commons license and your intended use is not permitted by statutory regulation or exceeds the permitted use, you will need to obtain permission directly from the copyright holder. To view a copy of this license, visit <http://creativecommons.org/licenses/by/4.0/>.

compared with melanocytes and normal tissue^{11–13}. Since *Grm1* is placed under the control of the melanocyte-specific *Dct* promoter in the Tg(*Grm1*) mouse model, *Grm1* is specifically overexpressed in cells of melanocytic origin leading to cutaneous as well as uveal melanoma^{11,14}. Further, in this mouse model the development of metastasis in lymph nodes, lung and liver were observed¹⁵.

Both angiogenesis and lymph angiogenesis, the formation of new blood or lymphatic vessels from pre-existing ones, are described as crucial processes in melanoma development and progression. It was shown that the induction of angiogenesis can be mediated by single transformed melanoma cells¹⁶. Further, the correlation between lymph angiogenesis and melanoma progression to distant metastases was described previously^{17,18}.

In this report, we demonstrate that *Cyld*-deficiency promotes melanoma onset and growth in the Tg(*Grm1*) mouse model. Furthermore, CYLD has an impact on cellular processes in vitro as it negatively regulates proliferation, migration and colony formation. In addition, we present data that indicate a new regulatory role of CYLD regarding vasculogenic mimicry and (lymph-) angiogenesis in malignant melanoma. Thus, our results confirm the Tg(*Grm1*) mouse model as a reliable model for further investigations regarding molecular processes in malignant melanoma. Finally, our new findings constitute a step forward in understanding the specific role of the tumor suppressor CYLD in malignant melanoma.

Results

Loss of CYLD accelerates melanoma onset and increases tumor growth in vivo

To study the role of CYLD in melanoma tumorigenesis in vivo, Tg(*Grm1*) mice¹¹ were crossbred with C57BL/6 *Cyld*-knockout mice¹⁹. The generated Tg(*Grm1*) *Cyld*^{+/+} and Tg(*Grm1*) *Cyld*^{-/-} mice were then analyzed for melanoma onset (Fig. 1a). Tg(*Grm1*) *Cyld*^{-/-} mice develop melanoma significantly earlier compared to the Tg(*Grm1*) *Cyld*^{+/+} control group. *Cyld*^{+/+} mice exhibited tumors 18 weeks after birth, whereas melanoma onset of *Cyld*^{-/-} mice was already observed after 10 weeks. Further, the progression of melanoma growth on ear, tail and anus were followed for nine weeks after tumor onset. Here, a scoring from minimal¹ to extreme tumor growth⁶ was used to quantify melanoma progression as described previously²⁰. This documentation revealed that *Cyld*-knockout mice display increased tumor growth compared to *Cyld*-wildtype mice (Fig. 1b). Additionally, the *Grm1* mRNA expression in lymph node tissues of Tg(*Grm1*) *Cyld*^{+/+} and Tg(*Grm1*) *Cyld*^{-/-} mice was analyzed as marker for melanoma cell dissemination. Here, a significantly enhanced *Grm1* expression at the age of 77d was observed in lymph nodes of the *Cyld*^{-/-} mice

whereas no melanoma cells were detected in *Cyld*^{+/+} mice (Supplementary Fig. S1).

RNA sequencing revealed CYLD-dependent gene regulation

In order to define CYLD-dependent deregulated genes and the underlying mechanism resulting in increased tumor growth in the *Cyld*-knockout mice, RNA sequencing was performed²¹. Here, primary tumor tissue from Tg(*Grm1*) *Cyld*^{+/+} versus Tg(*Grm1*) *Cyld*^{-/-} was used to determine the gene expression profile (p -value < 0.05; $0.66 < FC > 1.5$; FC = foldchange). RNA sequencing revealed 398 upregulated and 101 downregulated genes in the *Cyld*-knockdown tissue compared to the wild-type tissue (data not shown). To identify an impact of deregulated genes on pathway regulation, the differentially expressed genes were analyzed in STRING and classified corresponding to GO terms. The classification of KEGG pathways revealed many pathways known to be deregulated in cancer, for example TGF-beta and Rap1 (Table 1). Here, we confirmed the upregulation of TGF-beta signaling in *Cyld*-knockout compared to *Cyld*-wildtype cell lines using Smad2/3-responsive reporter gene assays (Supplementary Fig. S2). This is in agreement with the differential expression of several TGF-beta target genes like BMP2K or SMURF1. Interestingly, the classification according to biological processes yields regulation of cell proliferation, migration and also angiogenesis (Table 2).

Generation of Tg(*Grm1*) melanoma cell lines

On the basis of the RNA sequencing results and to gain further insight into how CYLD acts as tumor suppressor in malignant melanoma, cell lines of both Tg(*Grm1*) *Cyld*-wildtype and Tg(*Grm1*) *Cyld*-knockout mice were generated. For this purpose, melanoma cells of primary melanoma tissue from tail and ear, as well as metastatic melanoma cells from the lymph node were isolated (Fig. 1c). As pigmentation was lost after a few passages in all cell lines (Fig. 1d), the melanocytic origin was confirmed by electron microscopy showing melanosomes in all tested cell lines (Fig. 1e). In addition, qRT-PCR analyses revealed a comparable *Grm1* mRNA expression level of cultivated Tg(*Grm1*) cell lines to murine cerebellum (positive control, set as 1), whereas the murine B16 melanoma and melanocytic Melan-A cell line (negative control) displayed extremely low *Grm1* expression (Fig. 1f). Moreover, GRM1 expression in the *Cyld*-wildtype and *Cyld*-knockout cell lines was comparable. This hints at the fact that the generated cells, with same genetic GRM1 background, carry and express the *Grm1* transgene controlled by the *Dct* promoter and therefore are of melanocytic origin. Furthermore, CYLD protein levels were confirmed by Western blot showing CYLD expression in

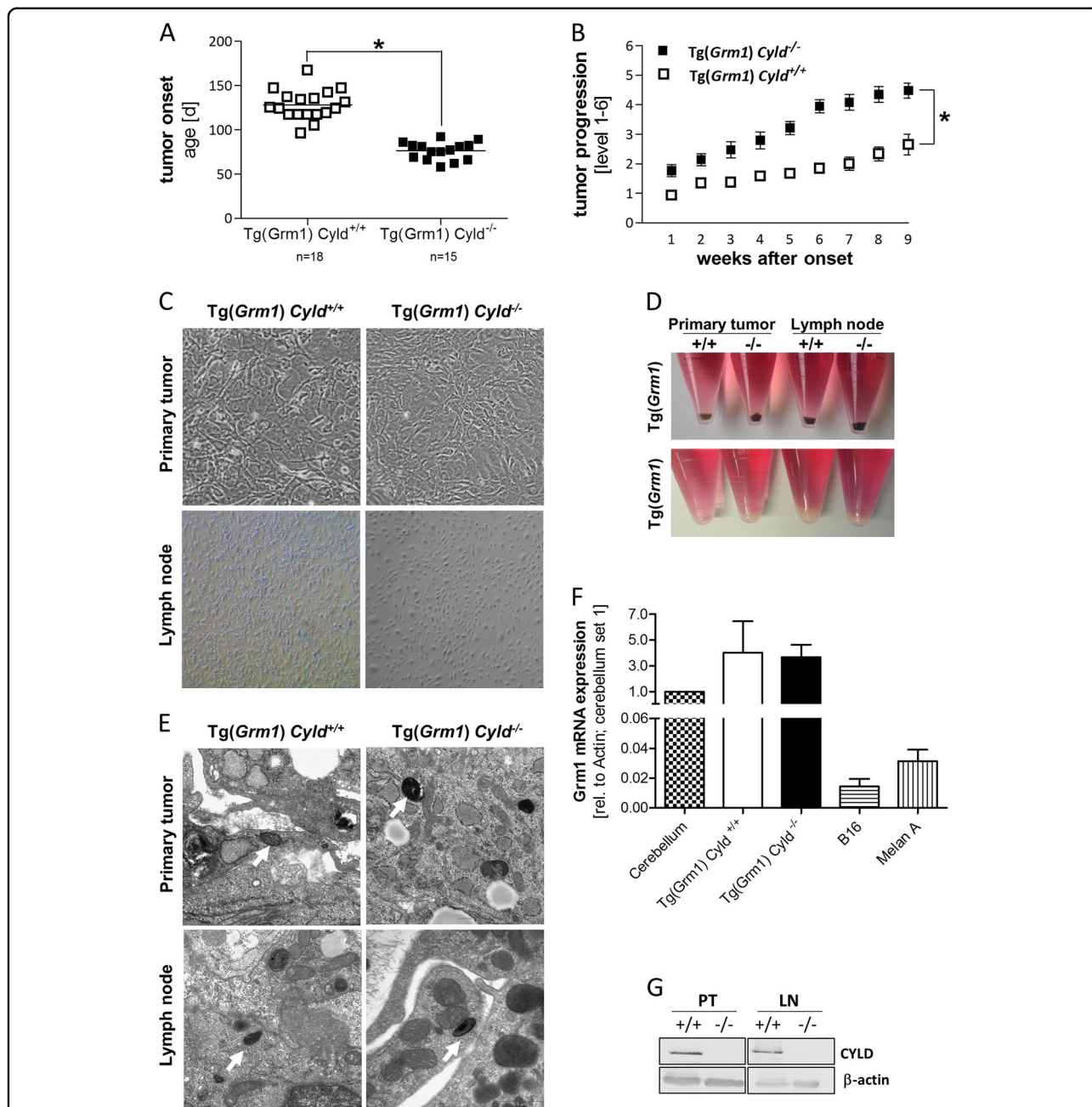


Fig. 1 Melanoma onset and progression in vivo and generation of *Tg(Grm1)* melanoma cell lines. **a** Melanoma onset in *Tg(Grm1) Cylid^{-/-}* ($n = 15$) and *Tg(Grm1) Cylid^{+/+}* mice ($n = 18$). **b** Tumor progression of the *Cylid*-knockout mice compared with *Cylid*-wildtype mice after tumor onset. The grading system to evaluate the progression of tumor growth at the tail, ear and perianal region for additional nine weeks after tumor onset has been applied as previously described¹⁹. **c** For cultivation of murine melanoma cell lines tissue of primary melanoma (ear and tail), as well as metastatic melanoma tissue (lymph node) was taken from *Tg(Grm1) Cylid^{+/+}* and *Tg(Grm1) Cylid^{-/-}* mice. **d** Loss of pigmentation of the cell lines was observed after a few passages. **e** Transmission electron microscopy analysis of spheroids from primary tumor cell line and metastatic cell line gained from *Cylid^{+/+}* and *Cylid^{-/-}* mice displayed melanosomes (arrow). **f** Quantification of *Grm1* mRNA expression of the generated *Tg(Grm1)* cell lines ($n = 10$) compared with murine cerebellum as control (set as 1) was measured via qRT-PCR analysis. MelanA and B16 were used as negative control and β -Actin served as reference gene. **g** CYLD protein level was measured via western blot to confirm the *Cylid* genotype. GAPDH was used as loading control. ($*p < 0.05$)

Table 1 KEGG pathway analysis via String database (p -value < 0,05; $0,66 < FC^a > 1.5$)

KEGG pathway description	Observed gene count	False discovery rate	Matching proteins in the network
ECM-receptor interaction	11	7.92E-04	Col11a1,Col27a1,Col4a6,Gp1bb,Itga2b,Itgb4,Lamb3, Sdc4,Thbs2,Thbs3,Tnxb
Hedgehog signaling pathway	8	1.23E-03	Bmp2,Bmp4,Gas1,Gli1,Wnt10a,Wnt3,Wnt4,Wnt7b
Retinol metabolism	9	4.55E-03	Adh1,Aldh1a7,Cyp1a1,Cyp2b10,Cyp2b19,Rdh12,Rdh16, Sdr16c5,Ugt1a1
TGF-beta signaling pathway	9	4.55E-03	Bmp2,Bmp4,Bmp7,Dcn,Fst,Id1,Id3,Id4,Nog
Hippo signaling pathway	12	5.13E-03	Bmp2,Bmp4,Bmp7,Id1,Lats2,Nkd1,Pard6b,Trp73,Wnt10a, Wnt3,Wnt4,Wnt7b
Tight junction	11	6.66E-03	Cgn,Cldn1,Cldn23,Cldn4,Crb3,Epb4.1l3,Gnai1,Myh14, OcIn,Pard6b,Tjp3
Basal cell carcinoma	7	6.66E-03	Bmp2,Bmp4,Gli1,Wnt10a,Wnt3,Wnt4,Wnt7b
Leukocyte transendothelial migration	10	9.90E-03	Arhgap5,Cldn1,Cldn23,Cldn4,Cxcl12,Gnai1,Mapk13,Msn, OcIn,Vcl
Steroid hormone biosynthesis	8	9.98E-03	Akr1c18,Cyp1a1,Cyp2b10,Cyp2b19,Cyp7b1,Hsd17b2, Hsd3b6,Ugt1a1
Histidine metabolism	5	9.98E-03	Aldh3a1,Aldh3b2,Aspa,Hal,Maob
Metabolism of xenobiotics by cytochrome P450	7	9.98E-03	Adh1,Aldh3a1,Aldh3b2,Cbr2,Cyp1a1,Cyp2f2,Ugt1a1
Arachidonic acid metabolism	8	1.21E-02	Alox12e,Cbr2,Cyp2b10,Cyp2b19,Cyp4f18,Fam213b, Ggt6,Ptgs1
Protein digestion and absorption	8	1.41E-02	Atp1a2,Col11a1,Col17a1,Col27a1,Col4a6,Cpa3,Fxyd2, Slc15a1
Amoebiasis	9	2.02E-02	Col11a1,Col27a1,Col4a6,Gna14,Il1r2,Lamb3,Serpinb13, Serpinb2,Vcl
Rap1 signaling pathway	12	3.60E-02	Adcy7,Efna3,Efna4,Fgfr2,Fgfr3,Gnai1,Id1,Itga2b,Lpar3, Mapk13,Pard6b,Rap1gap

^afoldchange**Table 2 GO analysis via String database**

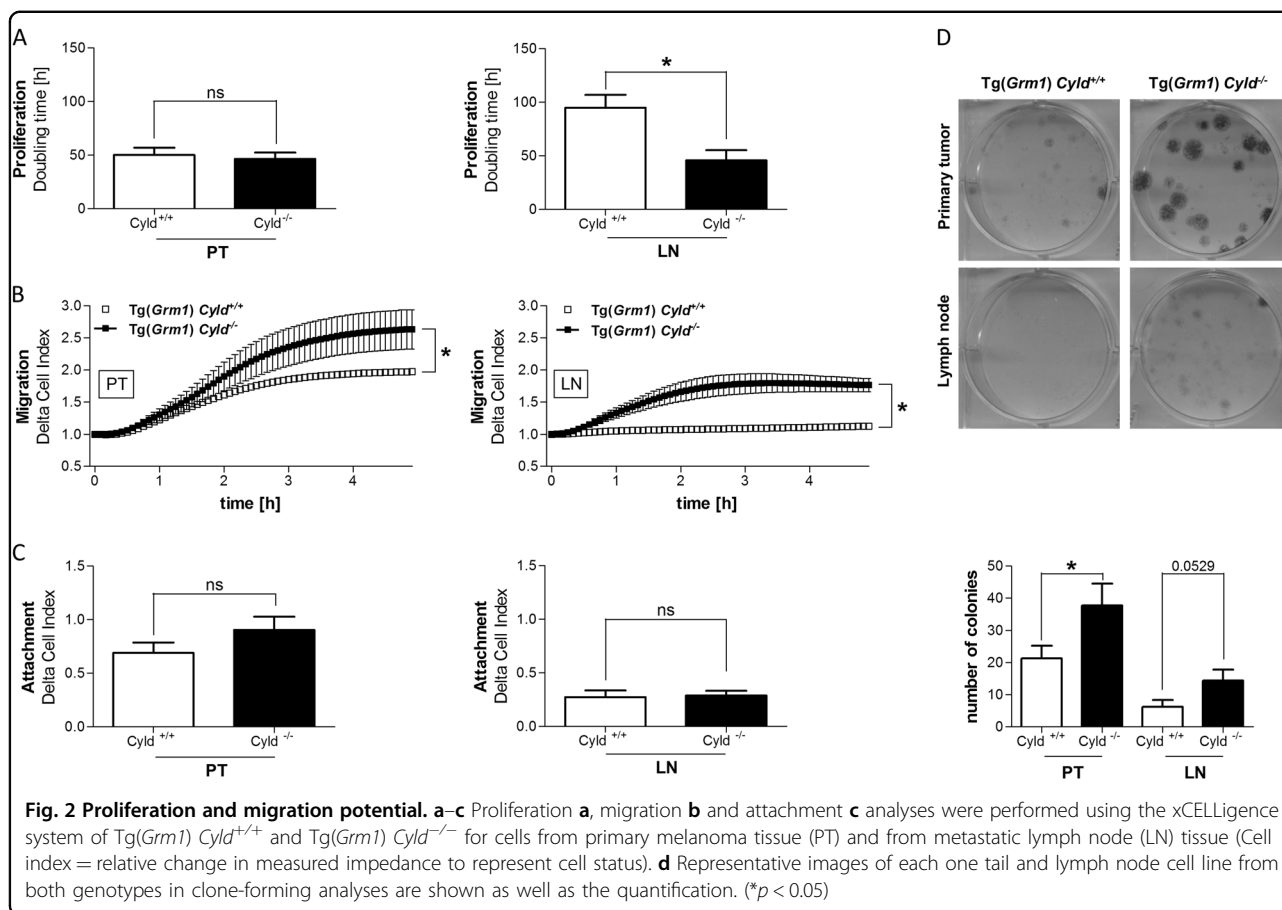
Term (GO number)	Observed gene count	False discovery rate
Regulation of cell proliferation (0042127)	64	4.32E-08
Regulation of cell migration (0030334)	28	1.39E-03
Regulation of angiogenesis (0045765)	12	2.47E-02

cell lines gained from *Cyld*-wildtype mice and no protein in *Cyld*-knockout mice (Fig. 1g).

***Cyld*-deficiency enhances proliferation, colony formation and migration**

After generating the melanoma cell lines out of tumors from Tg(*Grm1*) *Cyld*-wildtype and Tg(*Grm1*) *Cyld*-knockout mice, the cell lines were characterized using

functional in vitro assays. First, proliferation was measured by in vitro real-time proliferation assay using the xCELLigence system. This analysis revealed that the metastatic Tg(*Grm1*) *Cyld*^{-/-} cells show a reduced doubling time in comparison to *Cyld*-expressing cells, whereas the proliferative potential from primary tumor cells with or without CYLD expression was comparable (Fig. 2a). Because of the high metastatic tendency of



melanoma cells, also the migratory potential was analyzed. Both, primary tumor and metastatic Tg(*Grm1*) *Cyld*^{-/-} cells display significantly increased migration compared to the cell lines derived from Tg(*Grm1*) *Cyld*^{+/+} mice (Fig. 2b), whereas cell attachment was not influenced by CYLD (Fig. 2c). Additionally, analyses of the clonogenic potential revealed an increased ability to form colonies from single cells of both primary tumor and metastatic *Cyld*-deficient Tg(*Grm1*) cells compared to *Cyld*^{+/+} cells (Fig. 2d).

Loss of CYLD increases vasculogenic mimicry and promotes (lymph-) angiogenesis

As vasculogenic mimicry is a well-known feature of melanoma, the impact of CYLD on melanoma cells to form vascular tubes was analyzed^{22,23}. Tube formation assays were performed with the murine cell lines from primary melanoma and melanoma metastasis (Fig. 3a). All Tg(*Grm1*) *Cyld*^{-/-} cell lines were able to build vascular structures, whereas only one of six Tg(*Grm1*) *Cyld*^{+/+} cell lines showed this ability. To characterize this interesting difference in more detail, we studied the influence of CYLD-deficiency on angiogenesis. Studies show that the expression of *Timp2* (tissue inhibitor of metalloproteinase

2), *Timp3* (tissue inhibitor of metalloproteinase 3) and *Adamts5* (a disintegrin-like and metalloproteinase with thrombospondin type 1 motif, 5) reduce angiogenesis in melanoma cells^{24–26}. Therefore, mRNA expression patterns of these anti-angiogenic markers were examined. Although differences are not significant, Tg(*Grm1*) *Cyld*^{-/-} cell lines display a weaker expression of each marker compared to Tg(*Grm1*) *Cyld*^{+/+} cells (Fig. 3b).

Besides blood vessel formation, especially lymph angiogenesis is of particular importance in melanoma progression. As melanoma cells metastasize predominantly via lymphatic vessels into lymph nodes or distant organs, we aimed at understanding the relevant factors modulated by CYLD in this process. First, we investigated the role of CYLD in the formation of lymphatic vessels via immunofluorescence staining on murine Tg(*Grm1*) *Cyld*^{+/+} and *Cyld*^{-/-} melanoma tissues using LYVE-1, a specific lymphatic endothelial marker (Fig. 3c). Quantitative analyses revealed a markedly higher number of lymphatic vessels in melanoma tissues of *Cyld*-deficient mice compared to *Cyld*-wildtype mice indicating that CYLD may represent a regulator in melanoma lymph angiogenesis. Quantitative RT-PCR analyses were used to examine the mRNA expression pattern of well-known

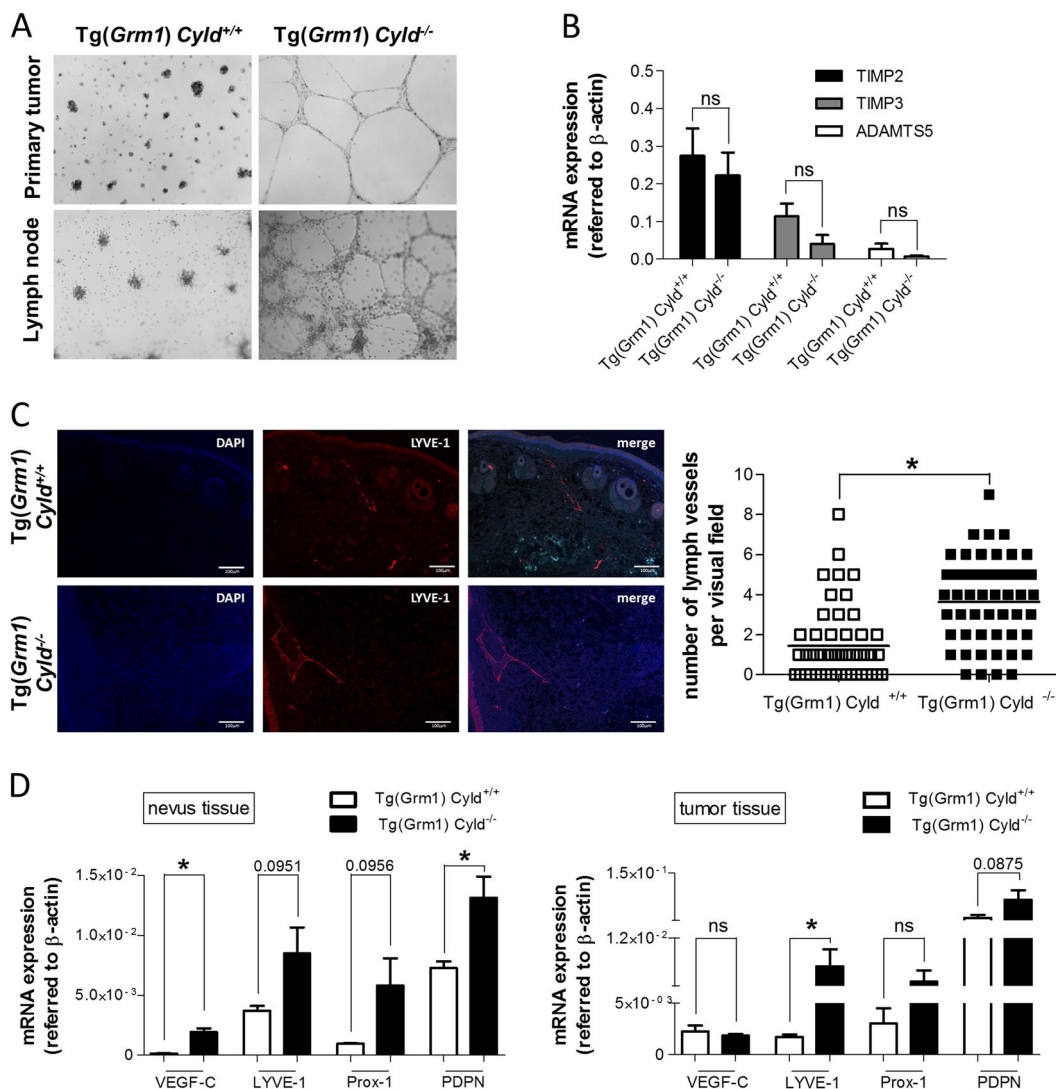


Fig. 3 CYLD loss enhances vasculogenic mimicry and (lymph-) angiogenesis. **a** Tube formation assays reveal an enhanced ability to form vascular structures in *Cyld*^{-/-} cells. **b** Via qRT-PCR analyses decreased mRNA expression of anti-angiogenic markers *Adamts5*, *Timp2* and *Timp3* was detected in *Cyld*-deficient cell lines compared to *Cyld*-wildtype cells. **c** LYVE-1 (red) immunofluorescence staining of *Tg(Grm1) Cylid*^{+/+} and *Tg(Grm1) Cylid*^{-/-} melanoma tail tissue. DAPI (blue) were used for nuclear staining. For quantification the number of lymphatic vessels was counted manually per visual field. **d** mRNA expression of lymph angiogenesis marker in nevus and tumor tissue. (**p* < 0.05)

lymph angiogenetic markers in nevus and tumor tissue of the model (Fig. 3d). This revealed an increased mRNA expression of VEGF-C, Podoplanin, LYVE-1 and Prox-1 in the nevus tissues *Cyld*-deficient mice. Although in tumor tissues only LYVE-1 expression is significantly upregulated, there is a notable tendency of higher expression of nearly all markers after loss of CYLD, which supports the role of CYLD in regulating lymph angiogenesis.

Discussion

In this study, a mouse model was newly developed to investigate the impact of CYLD deficiency on melanoma.

The model was generated on the background of the *Tg(Grm1)* melanoma mouse model showing spontaneous melanoma development¹¹. CYLD is known to have a tumor-suppressive role in human melanoma. Previous studies, including studies from our group, were able to link loss of CYLD to increased proliferation and invasion in vitro and tumor progression in vivo^{5,7}. However, its role in melanoma migration seems to be contradictory. Whereas some publications reported a diminished migratory potential upon *CYLD* re-expression in human melanoma cell lines^{5,7}, one study described a reduced migration when *CYLD*-expressing melanoma cells were treated with siRNA against *CYLD*⁶. Moreover, the

function of CYLD in metastasis is poorly examined and related processes, as lymph angiogenesis, were not analyzed previously.

Consistent with the strong differences in melanoma development in the *Cyld*-deficient and wildtype mice, RNA sequencing analysis revealed many deregulated genes in *Cyld*-deficient melanoma tissue. A study from Lim et al. demonstrated that CYLD acts as a negative regulator via inhibition of TGF- β signaling in fibrosis²⁷. The connection between CYLD and TGF- β signaling, observed by STRING analyses of the RNA-seq data, was confirmed by showing higher TGF- β pathway activity and increased expression of SMAD target genes (e.g. Bmp2k and Smurf1) in *Cyld*-knockout versus *Cyld*-wildtype cells and tissues. STRING analyses further confirmed the relevance of CYLD in the regulation of proliferation and migration as it was described already in human melanoma⁵. However interestingly, it also provided the first hints of an important role of CYLD in angiogenesis, the formation of new blood vessels from preexisting ones.

In line with the RNA sequencing data, in vitro studies with newly generated Tg(Grm1) melanoma cell lines displayed an enhanced proliferation, migration and clonogenicity in *Cyld*-knockout cell lines. These data are in agreement with previously published results gained from human melanoma cell lines and also demonstrate that the generated cell lines are a valid model for future studies of the tumor suppressor functions of CYLD^{5,7}.

Angiogenesis is a well-studied process in melanoma that helps the tumor to ensure the supply with nutrients and oxygen and promotes metastasis. Several angiogenic serum factors are elevated in melanoma patients²⁸ and high rate of angiogenesis correlates with poor prognosis for melanoma patients. Melanoma cells are known to have the intrinsic capacity of vascular mimicry²⁹. In this study, we revealed that CYLD has a regulatory role in vasculogenic mimicry of melanoma cells by suppressing tubular formation. Contradictory, a study from Gao et al. showed that the knockdown of CYLD expression impairs endothelial tube formation and sprouting of endothelial cells³⁰. This difference hints to a specific function of CYLD in different cell types and supports a role of CYLD in vascular mimicry of melanoma cells.

Our data indicate that loss of CYLD contributes to angiogenesis in melanoma by a potential negative effect on expression of several anti-angiogenic factors like TIMP-2, TIMP-3 and ADAMTS5. TIMP3 is described as an antagonist of VEGF-mediated angiogenesis²⁵ and ADAMTS5 was found to inhibit endothelial cell tube formation³¹. TIMP2 was shown to reduce the tube formation ability of the murine melanoma cell line B16²⁴. Moreover, in esophageal carcinoma TIMP-2 expression is negatively correlated with lymph node metastasis via inhibition of MMPs³².

Interestingly, the re-expression of a catalytically inactive form of CYLD (CYLD^{C/S}) compared to the wildtype CYLD re-expression did not result in decreased level of angiogenic factors, including VEGF-A³³. Moreover, only the overexpression of CYLD in comparison to CYLD^{C/S} reduced angiogenesis in human squamous cell carcinomas³⁴. Therefore, it seems that the deubiquitinase function of CYLD is important for the regulation of angiogenesis. This is supported by a study showing that CYLD acts in the process of trans-differentiation of adventitial fibroblasts via its deubiquitinase function and thus plays a role in vascular remodeling³⁵.

We, further, asked whether CYLD also influences the formation of lymphatic structures. In previous studies, the marker LYVE-1 was established to show that a high number of lymphatic vessels is prognostic for lymph node metastasis and metastasis in general. Further, an increased lymph vessel quantity is associated with poor outcome^{36–38}. Interestingly, melanoma tissue of *Cyld*-knockout mice exhibits more LYVE-1 positive vessels than the control group, thus CYLD is involved in the process of lymph angiogenesis. This is further corroborated by the observation that *Cyld*-deficiency enhances the expression of several established lymph angiogenesis markers³⁹. Remarkably, in our study already the benign nevus tissue of *Cyld*-deficient mice showed significantly enhanced expression of almost all investigated markers. Based on our results, loss of CYLD positively affects the formation of lymph vessels in melanoma and enhances metastasis, supporting the important role of CYLD especially in the early process of melanoma progression. In the context of angiogenesis and lymph angiogenesis, the analyses of the RNA sequencing data via STRING further supported the role of CYLD in these processes. Several cancer related pathways and processes differentially regulated in the sequencing data are known for their relevance in the formation of blood and lymph vessels. Here, also the in vitro data provided strong evidence that *Cyld*-deficiency promotes expression of several genes and signaling pathways that were already described to be involved in the process of angiogenesis as well as in lymph angiogenesis. All these findings support our hypothesis of the important role of CYLD in lymph-/angiogenesis.

In summary, the newly generated mouse model and the resulting cell lines of primary tumors and metastases represent a good base for studies of the function of CYLD in malignant melanoma. Here, a novel function for CYLD in both vasculogenic mimicry and lymph angiogenesis in melanoma was characterized. Furthermore, our findings demonstrate the crucial impact of CYLD on melanoma onset, progression and metastasis, as well as its multiple tumor-suppressive functions.

Material & methods

Mice

The transgenic Tg(*Grm1*) mice¹¹ were established at the Department of Chemical Biology, Rutgers University, Piscataway, USA and provided by Prof. Chen and Prof. Becker. C57Bl/6J *Cyld*-knockout mice¹⁹ were provided by Dr. Massoumi (Department of Laboratory Medicine, Lund University, Sweden). Mice were kept under standard conditions at 21 °C (± 1 °C) with 55% (± 10 %) relative humidity and 12 h light/dark intervals. Animals were fed with standard chow (Ssniff, Soest, Germany) and with drinking water *ad libitum*. Animal care and experimental procedures were carried out in accordance with the guidelines of the German law governing animal care. Experiments were approved by the Ethics Committee for Animal Research of the Bavarian government. For all analyses, homozygous transgenic Tg(*Grm1*) *Cyld*^{+/+} and Tg(*Grm1*) *Cyld*^{-/-} animals (litter mates) were used. For analyzing metastasis in the lymph nodes, mRNA from lymph node tissues was isolated as previously described and qRT-PCR for *Grm1* normalized on β -actin was performed⁴⁰.

Cell culture

Tg(*Grm1*) melanoma cell lines were generated, as previously described¹⁴. They were cultivated in DMEM containing 4500 mg glucose/l, 110 mg sodium pyruvate/l and l-glutamine and supplemented with 10% fetal bovine serum, amphotericin B (2.5 μ g/ml) and 5% penicillin/streptomycin (all from Sigma-Aldrich, München, Germany). Cell lines were incubated in a humidified atmosphere containing 8% CO₂ at 37 °C. Growth medium was renewed twice a week and cells were spilt at a ratio 1:3 to 1:5 once weekly.

Clonogenic assay

For clonogenic forming assays 250 cells were seeded in a well of a six-well plate. After an incubation time of ten days at 37 °C and 8% CO₂ cells were rinsed with PBS. Subsequently, colonies were fixed with 6% v/v glutaraldehyde and stained with crystal violet as described elsewhere⁴¹. Quantity of colonies was determined manually.

Cell migration and proliferation assays

In order to study the migratory and proliferative potential of Tg(*Grm1*) cells, the xCELLigence System was used (Roche, Mannheim, Germany)^{14,42–44}. This instrument monitors the behavior of the cells in real time by measuring the electrical impedance across interdigitated microelectrodes covering the bottom of the plates⁴³. The software calculates the cell index, a relative and dimensionless parameter of the electrode impedance to represent cell status. For migration analysis 2×10^4 cells in

100 μ l DMEM medium without FCS were seeded into the upper chambers of CIM-plates (similar to Boyden chamber) and were measured for 8 h. For attachment and proliferation experiments 2×10^3 and 4×10^3 cells in 100 μ l medium were seeded into E-Plates and electrical impedance was measured during 4 h and 90 h, respectively. Each cell line was measured in duplicate in two independent experiments.

Matrigel tube formation assay

For tube formation assays 200 μ l matrigel was added into each well of a eight-chamber culture slide (both from BD Biosciences, Bedford, USA). After polymerization at 37 °C murine Tg(*Grm1*) melanoma cells were seeded into each well in a total volume of 400 μ l DMEM high glucose medium (Sigma-Aldrich, Munich, Germany). Tube formation was photographically documented after 16 h incubation at 37 °C using an IX83 microscope (Olympus, Tokyo, Japan).

Transmission electron microscopy

For electron microscopy Tg(*Grm1*) cells were prepared as follows: 8×10^3 cells were seeded in 100 μ l medium in one well of a 96-well plate coated with 1% agarose to form spheroids. After an incubation time of three days at 37 °C spheroids were rinsed with PBS and fixed in 2.5% glutaraldehyde for 2 h at 4 °C. After a further washing step with PBS spheroids were postfixed in osmium tetroxide, embedded in Epon according to standard protocols and ultrathin sections were examined in a Zeiss 906 electron microscope (Zeiss, Oberkochen, Germany).

RNA isolation, Reverse Transcription and Quantitative RT-PCR

Total RNA was isolated using the E.Z.N.A. MicroElute Total RNA Kit (Omega Bio-Tek, VWR Darmstadt, Germany) according to the manufacturer's instructions. RNA concentration was measured with a NanoDrop spectrophotometer (PqLab Biotechnology GmbH, Erlangen, Germany) and cDNA was generated by reverse transcription using the Super Script II Reverse Transcriptase Kit (Life Technologies, Carlsbad, USA) with each reaction containing 500 ng of total RNA. Analysis of mRNA expression was performed using quantitative Real-Time PCR on the LightCycler 480 system (Roche, Mannheim, Germany). A volume of 1 μ l cDNA template, 0.5 μ l of forward and reverse primers (each 20 μ M) and 10 μ l of SYBR Green I (Roche, Mannheim, Germany) were combined to a total volume of 20 μ l. The following primers were used: *Adams5* for 5'-GCCATTGTAATAACC CTGCACC-3'; *Adams5* rev 5'-TCAGTCCCATCCGTA ACCTTTG-3'; β -Actin for 5'-TGGAATCCTGTGGCA TCCATGAAAC-3'; β -Actin rev 5'-TAAAACGCAGC TCAGTAACAGTCCG-3'; *Grm1* for 5'-GGGCAGG

GAACGCCAATTCT-3'; Grm1 rev 5'-TGGAAG GGCTGCTGGGAGGG-3'; Timp2 for 5'-GCAGACG TAGTGATCAGAGCC-3'; Timp2 rev 5'-TCCCAGGGC ACAATGAAGTC-3'; Lyve-1 for 5'-ACAGTGTGACA TTTGCCCT-3'; Lyve-1 rev 5'-CAGCCACACT CCGCTATAC-3'; PDPN for 5'-GTGCTACTGGAGG GCTTAATGA-3'; PDPN rev 5'-TGTTGTCT GCGTTTCATCCCC-3'; Prox-1 for 5'-GAGATGTGTG AGCTGGACCC-3'; Prox-1 rev 5'-CCTGAGGAA CCTGGCGAGAG-3'; VEGF-C for 5'-CTTCTTGT CTCTGGCGTGTTC-3'; VEGF-C rev 5'-GGTACA GGACAGACATCAGCTC-3'; Timp3 for 5'-GACC CTTGGCCACTTAGTCC-3' and Timp3 rev 5'-CGGA TCACGATGTCGGAGTTG-3'. Each sample was analyzed in duplicates. The target cDNA was normalized to β -Actin levels.

Protein isolation and Western blotting

Cells were lysed in 200 μ l RIPA buffer (Roche, Mannheim, Germany) for 15 min on 4 °C and thereafter the cell debris was separated via centrifugation at 13,000 rpm and 4 °C for 10 min. Protein concentration was determined using the Pierce BCA Protein Assay Kit (Thermo Fisher Scientific, Rockford, USA). In total 40 μ g of total lysate per lane were separated on 10% SDS-PAGE gels and subsequently transferred onto a PVDF membrane. After blocking for 1 h with 5% BSA/TBS-T the membrane was incubated overnight (4 °C) with one of the following antibodies: anti-GAPDH (Cell Signaling Technology, Frankfurt a.M.; 1:1000) or CYLD (Cell Signaling Technology, Frankfurt a.M.; 1:1000). After washing the membrane three times with TBS-T an incubation step followed for 1 h with the alkaline phosphate-coupled secondary antibody anti-rabbit AP (Cell Signaling Technology, 1:4000). Finally, the membrane was washed again for three times in TBS-T and the immunoreaction was then visualized using NBT/BCIP (Life technologies, Carlsbad, USA).

Immunofluorescence

For immunofluorescence staining of tissue samples 5 μ m sections of formalin-fixed and paraffin-embedded tissue blocks were used and treated, as described previously¹⁴. The incubation with the anti-LYVE-1 antibody (Abcam, Cambridge; 1:100 in 2% BSA/TBS) occurred overnight at 4 °C and after three washing steps with PBS the secondary antibody Alexa fluor 488 anti-rabbit (Life technologies, Carlsbad, USA; 1:500 in PBS) was added for 1 h at 37 °C. Finally, tissue sections were washed again with PBS and VECTASHIELDTM Slide Mounting Medium with DAPI (Vector Laboratories Inc., Burlingame, USA) was added for mounting. Photographic documentation was performed using the Axio Imager Zeiss Z1 microscope (Axiovision, Carl Zeiss, Oberkochen, Germany).

Luciferase reporter gene assay

The tumor cell lines (150,000 cells/well) were seeded into six-well plates and transiently transfected with 1 μ g plasmids (p(CAGA)₉ LUC⁴⁵, pGL2basic) using the lipofectamine plus method (Invitrogen) according to the manufacturer's instructions. For normalization of the transfection efficiency 0.1 μ g of a pRL-TK plasmid (Promega, Mannheim, Germany) was co-transfected. After 24 h of transfection the cells were harvested. The lysate was analyzed for luciferase activity with a luminometer using Promega dual-luciferase assay reagent⁴⁶.

RNA sequencing

Sample processing was performed at an Affymetrix Service Provider and Core Facility, "KFB - Center of Excellence for Fluorescent Bioanalytics" (Regensburg, Germany; www.kfb-regensburg.de)²¹. For the identification of known and predicted protein-protein interactions, STRING (Search Tool for the Retrieval of Interacting Genes/Proteins) database was used⁴⁷.

Statistical analysis

Results are shown as the mean \pm standard error of the mean or percent and statistical significance was determined using the Student's unpaired *t*-test calculated with the software GraphPad Prism (GraphPad Software, Inc., San Diego, USA). A *p*-value < 0.05 was considered as statistically significant (ns: not significant, **p* < 0.05).

Acknowledgements

We thank Prof. Suzie Chen (Rutgers University, Chemical Biology, Piscataway, USA) and Prof. Jürgen Becker (Medical University of Graz, Department of General Dermatology, Graz, Austria) for providing Tg(*Grm1*) animals, Dr. Ramin Massoumi (Department of Laboratory Medicine, Lund University, Sweden) for providing C57Bl/6 *Cyld*^{-/-} mice and Andrea Hilpert (Institute for Anatomy, Erlangen, Germany) for transmission electron microscopy. This study was supported by the German Research Foundation (DFG FOR2127).

Conflict of interest

The authors declare that they have no conflict of interest.

Publisher's note

Springer Nature remains neutral with regard to jurisdictional claims in published maps and institutional affiliations.

Supplementary Information accompanies this paper at (<https://doi.org/10.1038/s41389-019-0169-4>).

Received: 5 June 2019 Revised: 24 September 2019 Accepted: 24 September 2019

Published online: 07 October 2019

References

1. Bignell, G. R. et al. Identification of the familial cylindromatosis tumour-suppressor gene. *Nat. Genet.* **25**, 160–165 (2000).
2. Wang, L. et al. The BRG1- and hBRM-associated factor BAF57 induces apoptosis by stimulating expression of the cylindromatosis tumor suppressor gene. *Mol. Cell Biol.* **25**, 7953–7965 (2005).

3. Hellerbrand, C. et al. Reduced expression of CYLD in human colon and hepatocellular carcinomas. *Carcinogenesis* **28**, 21–27 (2007).
4. Zhong, S., Fields, C. R., Su, N., Pan, Y. X. & Robertson, K. D. Pharmacologic inhibition of epigenetic modifications, coupled with gene expression profiling, reveals novel targets of aberrant DNA methylation and histone deacetylation in lung cancer. *Oncogene* **26**, 2621–2634 (2007).
5. Massoumi, R. et al. Down-regulation of CYLD expression by Snail promotes tumor progression in malignant melanoma. *J. Exp. Med.* **206**, 221–232 (2009).
6. Ishikawa, Y. et al. Downregulation of cylindromatosis gene, CYLD, confers a growth advantage on malignant melanoma cells while negatively regulating their migration activity. *Int. J. Oncol.* **41**, 53–60 (2012).
7. Ke, H. et al. CYLD inhibits melanoma growth and progression through suppression of the JNK/AP-1 and beta1-integrin signaling pathways. *J. Invest. Dermatol.* **133**, 221–229 (2013).
8. Brummelkamp, T. R., Nijman, S. M., Dirac, A. M. & Bernards, R. Loss of the cylindromatosis tumour suppressor inhibits apoptosis by activating NF-kappaB. *Nature* **424**, 797–801 (2003).
9. Reiley, W., Zhang, M. & Sun, S. C. Negative regulation of JNK signaling by the tumor suppressor CYLD. *J. Biol. Chem.* **279**, 55161–55167 (2004).
10. Tauriello, D. V. et al. Loss of the tumor suppressor CYLD enhances Wnt/beta-catenin signaling through K63-linked ubiquitination of Dvl. *Mol. Cell.* **37**, 607–619 (2010).
11. Pollock, P. M. et al. Melanoma mouse model implicates metabotropic glutamate signaling in melanocytic neoplasia. *Nat. Genet.* **34**, 108–112 (2003).
12. Namkoong, J. et al. Metabotropic glutamate receptor 1 and glutamate signaling in human melanoma. *Cancer Res.* **67**, 2298–2305 (2007).
13. Lee, H. J., Wall, B. A., Wangari-Talbot, J. & Chen, S. Regulation of mGluR1 expression in human melanocytes and melanoma cells. *Biochim. Biophys. Acta* **1819**, 1123–1131 (2012).
14. Schiffner, S. et al. Tg(Grm1) transgenic mice: a murine model that mimics spontaneous uveal melanoma in humans? *Exp. Eye Res.* **127**, 59–68 (2014).
15. Schiffner, S., Chen, S., Becker, J. C. & Bosserhoff, A. K. Highly pigmented Tg (Grm1) mouse melanoma develops non-pigmented melanoma cells in distant metastases. *Exp. Dermatol.* **21**, 786–788 (2012).
16. Schaafhausen, M. K. et al. Tumor angiogenesis is caused by single melanoma cells in a manner dependent on reactive oxygen species and NF-kappaB. *J. Cell Sci.* **126**, 3862–3872 (2013).
17. Pereira, M. A. et al. Risk factors for lymph node metastasis in western early gastric cancer after optimal surgical treatment. *J. Gastrointest. Surg.* **22**, 23–31 (2018).
18. Ma, Q. et al. Unexpected contribution of lymphatic vessels to promotion of distant metastatic tumor spread. *Sci. Adv.* **4**, eaat4758 (2018).
19. Massoumi, R., Chmielarska, K., Henneke, K., Pfeifer, A. & Fassler, R. Cylid inhibits tumor cell proliferation by blocking Bcl-3-dependent NF-kappaB signaling. *Cell* **125**, 665–677 (2006).
20. Stieglitz, D. et al. BMP6-induced modulation of the tumor micro-milieu. *Oncogene* **38**, 609–621 (2019).
21. de Jel, M. M. et al. Transcriptome sequencing of melanocytic nevi and melanomas from Grm1 transgenic mice to determine melanoma driver mutations. *Pigment Cell Melanoma Res.* **27**, 678–680 (2014).
22. Rothhammer, T., Bataille, F., Spruss, T., Eissner, G. & Bosserhoff, A. K. Functional implication of BMP4 expression on angiogenesis in malignant melanoma. *Oncogene* **26**, 4158–4170 (2007).
23. Hendrix, M. J. et al. Tumor cell vascular mimicry: novel targeting opportunity in melanoma. *Pharm. Ther.* **159**, 83–92 (2016).
24. Valente, P. et al. TIMP-2 over-expression reduces invasion and angiogenesis and protects B16F10 melanoma cells from apoptosis. *Int. J. Cancer* **75**, 246–253 (1998).
25. Qi, J. H. et al. A novel function for tissue inhibitor of metalloproteinases-3 (TIMP3): inhibition of angiogenesis by blockage of VEGF binding to VEGF receptor-2. *Nat. Med.* **9**, 407–415 (2003).
26. Kumar, S., Sharghi-Namini, S., Rao, N. & Ge, R. ADAMTS5 functions as an anti-angiogenic and anti-tumorigenic protein independent of its proteoglycanase activity. *Am. J. Pathol.* **181**, 1056–1068 (2012).
27. Lim, J. H. et al. CYLD negatively regulates transforming growth factor-beta signalling via deubiquitinating Akt. *Nat. Commun.* **3**, 771 (2012).
28. Ugurel, S., Rapp, G., Tilgen, W. & Reinhold, U. Increased serum concentration of angiogenic factors in malignant melanoma patients correlates with tumor progression and survival. *J. Clin. Oncol.* **19**, 577–583 (2001).
29. Maniotis, A. J. et al. Vascular channel formation by human melanoma cells in vivo and in vitro: vasculogenic mimicry. *Am. J. Pathol.* **155**, 739–752 (1999).
30. Gao, J. et al. CYLD regulates angiogenesis by mediating vascular endothelial cell migration. *Blood* **115**, 4130–4137 (2010).
31. Sharghi-Namini, S. et al. The first but not the second thrombospondin type 1 repeats of ADAMTS5 functions as an angiogenesis inhibitor. *Biochem. Biophys. Res. Commun.* **371**, 215–219 (2008).
32. Yang, X. et al. Influence of lymphatic endothelial cells on proliferation and invasiveness of esophageal carcinoma cells in vitro and lymphangiogenesis in vivo. *Med. Oncol.* **32**, 222 (2015).
33. Alameda, J. P. et al. An inactivating CYLD mutation promotes skin tumor progression by conferring enhanced proliferative, survival and angiogenic properties to epidermal cancer cells. *Oncogene* **29**, 6522–6532 (2010).
34. Alameda, J. P. et al. CYLD regulates keratinocyte differentiation and skin cancer progression in humans. *Cell Death Dis.* **2**, e208 (2011).
35. Yu, B. et al. CYLD deubiquitinates nicotinamide adenine dinucleotide phosphate oxidase 4 contributing to adventitial remodeling. *Arterioscler Thromb. Vasc. Biol.* **37**, 1698–1709 (2017).
36. Dadrás, S. S. et al. Tumor lymphangiogenesis predicts melanoma metastasis to sentinel lymph nodes. *Mod. Pathol.* **18**, 1232–1242 (2005).
37. Dadrás, S. S. et al. Tumor lymphangiogenesis: a novel prognostic indicator for cutaneous melanoma metastasis and survival. *Am. J. Pathol.* **162**, 1951–1960 (2003).
38. Shields, J. D. et al. Lymphatic density and metastatic spread in human malignant melanoma. *Br. J. Cancer* **90**, 693–700 (2004).
39. Jackson, D. G. Lymphatic markers, tumour lymphangiogenesis and lymph node metastasis. *Cancer Treat. Res.* **135**, 39–53 (2007).
40. Schott, M. et al. Selenium-binding protein 1 is down-regulated in malignant melanoma. *Oncotarget* **9**, 10445–10456 (2018).
41. Franken, N. A., Rodermond, H. M., Stap, J., Haveman, J. & van Bree, C. Clonogenic assay of cells in vitro. *Nat. Protoc.* **1**, 2315–2319 (2006).
42. Kwon, H. K., Lee, J. H., Shin, H. J., Kim, J. H. & Choi, S. Structural and functional analysis of cell adhesion and nuclear envelope nano-topography in cell death. *Sci. Rep.* **5**, 15623 (2015).
43. Braig, S. & Bosserhoff, A. K. Death inducer-obliterator 1 (Dido1) is a BMP target gene and promotes BMP-induced melanoma progression. *Oncogene* **32**, 837–848 (2013).
44. Xhernalce, B., Robson, S. C. & Kouzarides, T. Human RNA methyltransferase BCDIN3D regulates microRNA processing. *Cell* **151**, 278–288 (2012).
45. Rothhammer, T. & Bosserhoff, A. K. Influence of melanoma inhibitory activity on transforming growth factor-beta signaling in malignant melanoma. *Melanoma Res.* **16**, 309–316 (2006).
46. Dietrich, P. et al. Wild type Kirsten rat sarcoma is a novel microRNA-622-regulated therapeutic target for hepatocellular carcinoma and contributes to sorafenib resistance. *Gut* **67**, 1328–1341 (2018).
47. Szklarczyk, D. et al. STRINGv10: protein-protein interaction networks, integrated over the tree of life. *Nucleic Acids Res.* **43**, D447–D452 (2015).